Al-Khwarizmi Engineering Journal, Vol. 7, No. 1, PP 56 - 75 (2011)

Al-Khwarizmi Engineering Journal

A Finite Element Analysis for the Damaged Rotating Composite Blade

Oday I. Abdullah

Department of Energy Engineering/ College of Engineering/ University of Baghdad

Email: Odayia2006@yahoo.com

(Received 4 January 2010; Accepted 4 April 2011)

Abstract

In this paper, the finite element method is used to study the dynamic behavior of the damaged rotating composite blade. Three dimensional, finite element programs were developed using a nine node laminated shell as a discretization element for the blade structure (the same element type is used for damaged and non-damaged structure). In this analysis the initial stress effect (geometric stiffness) and other rotational effects except the carioles acceleration effect are included. The investigation covers the effect speed of rotation, aspect ratio, skew angle, pre-twist angle, radius to length, layer lamination and fiber orientation of composite blade. After modeling a non-damaged rotating composite blade, the work procedure was to apply different damage cases in reference to the non-damaged structure in order to compute the shift in the fundamental natural frequency and stresses. Damage occurs in several layers of the composite sheet in different locations throughout its volume, and through several layers of the sheet. The numerical results show a good agreement compared with the available investigations using other methods.

Keywords: *Damaged rotating blade, composite materials, FEM, stresses and frequencie.*

1. Introduction

Blades are key structural units in turbo-machinery of the aeronautical and aerospace industries. In the operational condition of the machinery, it is required to investigate the vibration characteristics of the rotating blades for design and analysis of efficient performance prediction and high specific strength etc. Thus, vibration analysis of turbo-machinery blades has received much attention for decades, and one can easily find numerous references of literature related to the eigen-frequency problems. Many research workers have assumed the turbomachinery blade as a beam which may be adequate for a blade with high aspect ratios. As a matter of fact, the chord-wise bending modes becomes involved in the vibration due to the effect of the decrease in the blade aspect ratio.

Omprakash and Ramamurti [1] carried out the steady-state, dynamic stress and deformation analysis of high pressure stage turbomachinery bladed discs taking into account all the geometric complexities involved and included the contributions due to initial stress and membrane behavior. They used a triangular shell element with six degrees of freedom per node.

Stephen and Wang [2] analyzed the rotating blade according to the theory of elasticity. The problem is reduced to a two-dimensional boundary value problem to which the stresses, strains, and displacements for a rotating blade having no pre-twist or taper were determined.

Leissa and Ewing [3] estimated the accuracy and limitation of the blade that is based on the beam theories. Furthermore, they pointed out that the beam theories are generally inadequate to determine the vibration frequencies and mode shapes of moderate to low aspect ratio models. During the recent years, a more rigorous method of analysis has been developed based on the plate theory.

Dokainish and Rawtani [4] investigated the natural frequencies and the mode shapes of a cantilevered plate mounted around a rotating disc.

They considered the chord-wise bending effects, and obtain accurate results. In addition,

Ramamurti and Kielb [5] predicted eigen frequencies of twisted rotating plates. Nowadays, shell type structures with different curvatures have been widely used as a part of turbomachines, which are the main feature relative to the beam and plate models. Thus, shell models are preferable to plate models due to the effect of surface curvature variation of the structures. Leissa and his coworkers did extensive researches that greatly help in assessing the vibration characteristics of shell type turbo-machinery blades [6–9]. With the variational approach a classical concept is employed, in which a shallow and thin shell theory is used as the starting point of the finite element formulation. Those methods in references can be used for analyzing blades with relatively small double curvatures accurately, but are inadequate for blades with large curvatures and twists.

Henry et al. [10] summarized the important literatures on the shell finite elements that were developed in decades. In addition, Ahmad et al. [11] introduced the concept of the continuum based degenerated shell element, and treated the shells of arbitrarily shapes without adopting complicated assumptions for specific shell theories. Because of the popularity of this concept due to simplicity in formulation, many research works have been developed to improve the behavior of the degenerated shell element. The geometric and material non-linear analysis of shells was extended by Ramm [12] and Bathe and Bolourchi [13].

Huang and Hinton [14] presented a new nine-node degenerated shell element, which adopts an enhanced interpolation to overcome the locking phenomenon. Lee and Han [15] investigated the vibration of plates and shells using the degenerated shell elements with the assumed natural strains. With advancements in aerospace technology, composite materials have been widely used in lightweight structures. Furthermore, composites show great potential in the design of turbo-machinery blades due to the advantages of strength, durability and weight of the materials.

Bhumbla et al. [16] studied the natural frequencies and mode shapes of spinning laminated composite plates.

Lam and Qian [17] investigated the free vibrations of thick cross-ply laminated composite cylindrical shells spinning with its axis based on the first order shear deformation theory. Also, Kumar and Palaninathan [18] studied the finite element analysis of laminated shells by using the degenerated shell element. They suggested four models for analyzing the laminated shell structures, and studied the numerical accuracy and computational efficiency of the models by comparing layer stresses and buckling loads. The main aim of the present study is the vibration analysis of an initially twisted rotating composite blade. A general formulation is derived for an initially twisted rotating shell structures including the effect of centrifugal force and Coriolis acceleration. The blade is assumed to be a moderately thick open circular cylindrical shell with the transverse shear deformation and rotary inertia effects, and is oriented arbitrarily with respect to the axis of rotation. Based on the concept of degenerated shell element with the Reissner–Mindlin's assumptions, the finite element method is used for solving the governing equations. In the numerical study, effects of various parameters are investigated: initial twisting angles, thickness to radius ratios, chord length ratios, layer lamination and fiber orientation of composite blades. Also, they are compared with the previous works and experimental data.

2. Formulation

2.1. Basic Assumptions

In this study, the assumptions are as follows,

(1) A straight line normal to the mid-surface before deformation remains straight after deformation, and the transverse shear deformation is considered.
(2) A stress component normal to the shell mid-surfaces is negligible.

2.2. Geometry and Deformation of Degenerated Shell

Fig.(1.a) shows the position vector X of a generic material point P in the unreformed configuration, and the unit nodal vectors and the coordinates adopted in this study are also presented.

The position vector X can be expressed as;

$$X = X_o + ze_3 \qquad \ldots(1)$$

where X_0 is the position vector of a point O on the shell mid-surface and e3 is the unit normal vector of the shell mid-surface.

Using the non-dimensional coordinate 1 with respect to the thickness h of the shell, Eq. (1) can be reduced as;

$$X = X_o + \zeta\left(\frac{h}{2}\right)e_3 \qquad \ldots(2)$$

Fig.(1.b) shows the mechanism of the deformation of the shell. As the line segment OP changes to OP0; then ze3 is rotated to the ze03 due to the deformation. Then the displacement vector U of a generic material point P may be expressed as;

$$U = U_o + \zeta U_\zeta \qquad \ldots(3)$$

Where $U_\zeta = \frac{h}{2}(e_3' - e_3)$

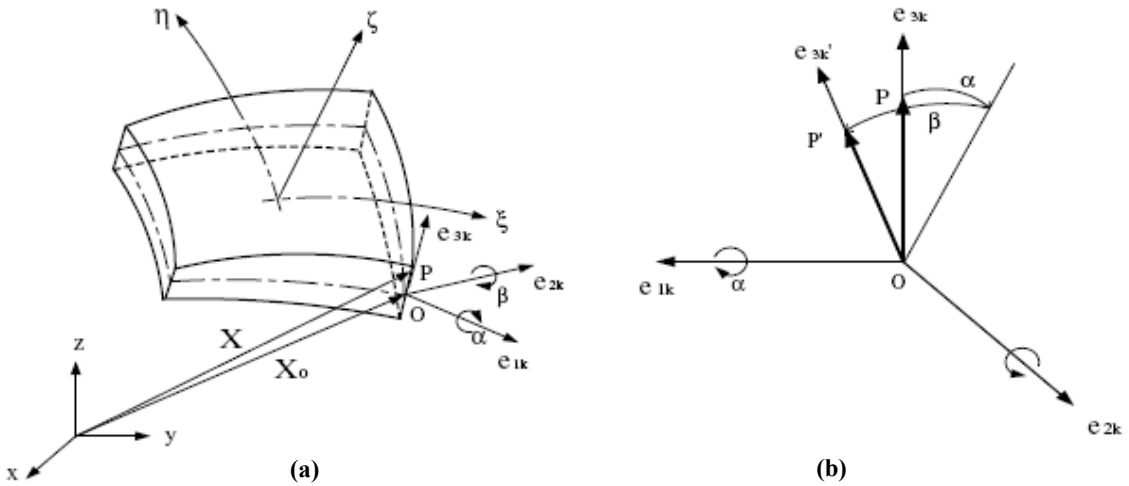

Fig.1. Geometry and Deformation Mechanism of the Degenerated Shell Element; (a) Geometry and Coordinate Systems, (b) Mechanism of Deformation.

In this study, the type of element is an isoparametric nine-node degenerated shell element. Five degrees of freedom are defined at each nodal point corresponding to its three translational displacement u_0, v_0, w_0 and two rotational degrees of freedom α, β.

As shown in Fig. (1.b), e_3' is described by the α rotation about e_1 and the β rotation about e_2. In this case, the positive sense of rotation angles α and β are defined with respect to the local coordinate system. Thus the displacement vector U_ζ can be expressed as,

$$U_\zeta = \frac{h}{2}[\sin\beta e_1 + \sin\alpha\cos\beta e_2 + (\cos\alpha\cos\beta - 1)e_3] \qquad \ldots(4)$$

For small deformation assumption, Eq. (4) can be simplified to

$$U_\zeta = \frac{t}{2}\begin{bmatrix} e_2^x & e_1^x \\ e_2^y & e_1^y \\ e_2^z & e_1^z \end{bmatrix}\begin{Bmatrix}\alpha \\ \beta\end{Bmatrix} \qquad \ldots(5)$$

2.3. Finite Element Formulation

The coordinate nodal values were used to interpolate the position and displacement vectors, and these vectors are expressed as follows,

$$\begin{Bmatrix} x \\ y \\ z \end{Bmatrix} = \sum_{i=1}^{9} N_i \begin{Bmatrix} x_i \\ y_i \\ z_i \end{Bmatrix}_{mid} + \zeta \sum_{i=1}^{9} N_i \frac{t_i}{2}\begin{Bmatrix} e_{3i}^x \\ e_{3i}^y \\ e_{3i}^z \end{Bmatrix} \qquad \ldots(6)$$

$$\begin{Bmatrix} u \\ v \\ w \end{Bmatrix} = \sum_{i=1}^{9} N_i \begin{Bmatrix} U_{oi} \\ v_{oi} \\ w_{oi} \end{Bmatrix}_{mid} + \zeta \sum_{i=1}^{9} N_i \frac{h_i}{2}\begin{bmatrix} e_{2i}^x & e_{1i}^x \\ e_{2i}^y & e_{1i}^y \\ e_{2i}^z & e_{1i}^z \end{bmatrix}\begin{Bmatrix}\alpha \\ \beta\end{Bmatrix} \qquad \ldots(7)$$

Eq. (7) can be simplified to

$$\begin{bmatrix} u & v & w \end{bmatrix}^T = N_q \qquad \ldots(8)$$

$$q = \begin{bmatrix} d_1 & d_2 & \ldots & d_i & \ldots & d_9 \end{bmatrix} \quad \text{and}$$

$$d_i = \begin{bmatrix} u_{oi} & v_{oi} & w_{oi} & \alpha_i & \beta_i \end{bmatrix}^T$$

also, N is the interpolation function matrix of the nine-node isoparametric element as shown below.

$$N = \begin{bmatrix} \overline{N}_1 & \overline{N}_2 & \ldots & \overline{N}_i & \ldots & \overline{N}_9 \end{bmatrix}$$

$$N_i = \begin{bmatrix} N_i & 0 & 0 & \varsigma N_i \frac{t}{2} e_{2i}^x & \varsigma N_i \frac{t}{2} e_{1i}^x \\ 0 & N_i & 0 & \varsigma N_i \frac{t}{2} e_{2i}^y & \varsigma N_i \frac{t}{2} e_{1i}^y \\ 0 & 0 & N_i & \varsigma N_i \frac{t}{2} e_{2i}^z & \varsigma N_i \frac{t}{2} e_{1i}^z \end{bmatrix} \quad (i=1,\ldots,9) \qquad \ldots(9)$$

For the case of a composite blade, the through thickness numerical integration is carried out by modifying the variable ς to ς_k in the k_{th} layer such that ς_k varies from -1 to 1 in that layer. Fig. (2) shows the nine node laminated shell element. The non-dimensional coordinate ς can be rewritten as:

$$\varsigma = -1 + \left[2\sum_{j=1}^{k} h_j - h_k(1-\varsigma_k) \right] / t \qquad \ldots(10)$$

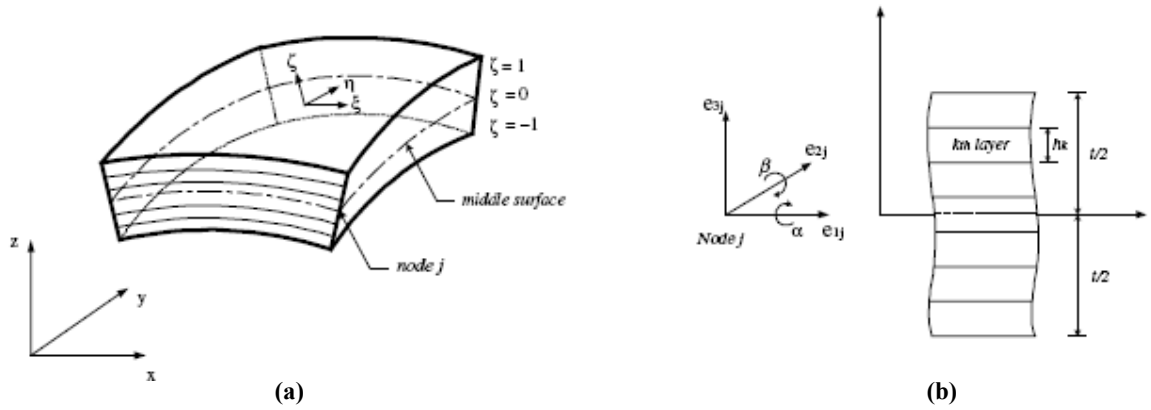

(a) **(b)**

Fig.2. Composite Lamination of the Degenerated Shell Element (a) Nine-Node Layered Curved Shell Element (b) Orthogonal Local Axes at a Shell Node j and Cross Section of Shell.

The covariant displacement components in the natural coordinate system are obtained by projecting the displacement components expressed in the global Cartesian coordinate system onto the natural coordinate directions which are expressed as;

$$u_\alpha = \frac{\partial x^i}{\partial \xi^k} u_i \qquad \ldots(11)$$

where repeated indices denote the summation (i=1, 2, 3, $\alpha = \xi, \eta, \varsigma$).

Eq. (11) can also be rewritten in a matrix form as;

$$\begin{Bmatrix} u_\xi \\ u_\eta \\ u_\varsigma \end{Bmatrix} = \begin{bmatrix} x_{,\xi} & y_{,\xi} & z_{,\xi} \\ x_{,\eta} & y_{,\eta} & z_{,\eta} \\ x_{,\varsigma} & y_{,\varsigma} & z_{,\varsigma} \end{bmatrix} \begin{Bmatrix} u \\ v \\ w \end{Bmatrix} = J \begin{bmatrix} u & v & w \end{bmatrix}^T \qquad \ldots(12)$$

Let

$$G = \begin{bmatrix} G_{,\xi} & G_{,\eta} & G_{,\varsigma} \end{bmatrix}^T \qquad \ldots(13)$$

Where

$$G_\xi = \begin{bmatrix} u_{,\xi} & v_{,\eta} & w_{,\varsigma} \end{bmatrix}^T, \quad G_\eta = \begin{bmatrix} u_{,\xi} & v_{,\eta} & w_{,\varsigma} \end{bmatrix}^T$$

and $G_\varsigma = \begin{bmatrix} u_{,\xi} & v_{,\eta} & w_{,\varsigma} \end{bmatrix}^T$

The strain vectors are composed by the following procedures;

$$\begin{bmatrix}\varepsilon_x & \varepsilon_y & \varepsilon_z & \gamma_{xy} & \gamma_{yz} & \gamma_{xz}\end{bmatrix}^T = H\begin{bmatrix}u_{,x} & u_{,y} & u_{,z} & v_{,x} & \dots & w_{,z}\end{bmatrix}^T \quad \dots(14)$$

Where,

$$\begin{Bmatrix}u_{,x}\\u_{,x}\\u_{,x}\\v_{,x}\\.\\.\\.\\w_{,x}\end{Bmatrix} = \begin{bmatrix}J^{-1} & 0 & 0\\0 & J^{-1} & 0\\0 & 0 & J^{-1}\end{bmatrix} \begin{Bmatrix}u_{,\xi}\\u_{,\eta}\\u_{,\varsigma}\\v_{,\xi}\\.\\.\\.\\w_{,\xi}\end{Bmatrix}$$

$$H = \begin{bmatrix}1&0&0&0&0&0&0&0&0\\0&0&0&0&1&0&0&0&0\\0&0&0&0&0&0&0&0&1\\0&1&0&1&0&0&0&0&0\\0&0&0&0&0&1&0&1&0\\0&0&1&0&0&0&1&0&0\end{bmatrix}$$

Then, the strain–displacement relationship takes the form as;

$$\varepsilon = HJ^{-1}Gq = B_{st}\,q, \quad \dots(15)$$

Where,

$$q = \begin{bmatrix}d_1 & d_2 & \dots & d_9\end{bmatrix}^T$$

And $$d_i = \begin{bmatrix}u_{oi} & v_{oi} & w_{oi} & \alpha_i & \beta_i\end{bmatrix}^T$$

The complete structural strain–displacement matrix B_{st} can be divided into B_m and B_s, which are independent of ς, and B_b which is linear in ς, so that matrix is written as;

$$B_{st} = B_m + B_s + \varsigma B_b \quad \dots(16)$$

The stress–strain relationship can be written in the global coordinate system as $\sigma = E\varepsilon$ or the local coordinate system as $\sigma' = E'\varepsilon'$. The global material property matrix E is obtained from local property matrix E' by using a coordinate transformation matrix T_ε such as;

$$E = T_\varepsilon^T\, E' T_\varepsilon \quad \dots(17)$$

The strain energy can be expressed as;

$$U = \frac{1}{2}\sum_{k=1}^{n}\int_V \varepsilon^T\, E_\varepsilon\, dV \quad \dots(18)$$

where n denotes the number of composite layers.

Fig. (3) shows the configuration of the rotating shell type blade, which is modeled in the present study. The reference coordinate system (i, j, k) is defined in terms of the angular velocity Ω. In addition, the global coordinate system (e_x, e_y, e_z) has the offset from the reference coordinate system by translation (h_i, h_j, h_k) and rotation $(\theta_i, \theta_j, \theta_k)$. Also, the twist of the blade can be expressed by the following coordinate transformation;

$$\begin{bmatrix}\bar{x} & \bar{y} & \bar{z}\end{bmatrix}^T = T_{tw}\begin{bmatrix}x & y & w\end{bmatrix}^T = \begin{bmatrix}1 & 0 & 0\\0 & \cos\psi & -\sin\psi\\0 & \sin\psi & \cos\psi\end{bmatrix}\begin{bmatrix}x & y & z^T\end{bmatrix} \quad \dots(19)$$

where T_{tw} is the coordinate transformation matrix for a blade twist, and $\begin{bmatrix}\bar{x} & \bar{y} & \bar{z}\end{bmatrix}$ is the transformed coordinates of the initially twisted blade. With rotational motion Ω, the velocity vector of any arbitrary point of the blade may be written as;

$$V = \frac{dr}{dt} + \Omega \times r \quad \dots(20)$$

Where,

$$r = \begin{bmatrix}h_i & h_j & h_k\end{bmatrix}\begin{Bmatrix}i\\j\\k\end{Bmatrix} + \begin{bmatrix}x+u & y+v & z+w\end{bmatrix}\begin{Bmatrix}e\\e_y\\e_z\end{Bmatrix}$$

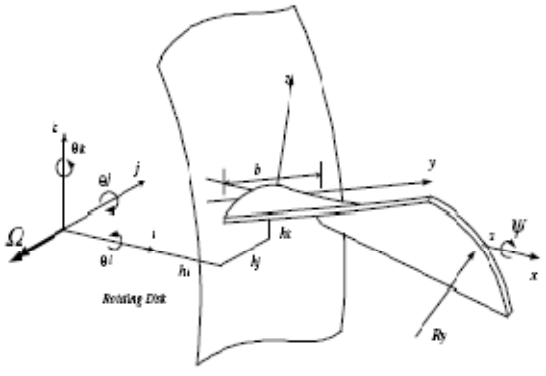

Fig.3. Rotating Blade Model with the Offsets (h_i, h_j, h_k) and Initial Twist (ψ).

The position vector r, defined in the reference coordinate system, can be obtained by using the global coordinate system (e_x, e_y, e_z) and reference coordinate system (I, j, k). The relationships between the two coordinate systems can be written as;

$$\begin{bmatrix} e_x & e_y & e_z \end{bmatrix}^T = T_L \begin{bmatrix} i & j & k \end{bmatrix}^T \quad \ldots(21)$$

Where,

$$T_L = \begin{bmatrix} \cos\theta_k & \sin\theta_k & 0 \\ -\sin\theta_k & \cos\theta_k & 0 \\ 0 & 0 & 1 \end{bmatrix} \begin{bmatrix} \cos\theta_j & 0 & -\sin\theta_j \\ 0 & 1 & 0 \\ \sin\theta_j & 0 & \cos\theta_j \end{bmatrix} \begin{bmatrix} 1 & 0 & 0 \\ 0 & \cos\theta_k & \sin\theta_k \\ 0 & -\sin\theta_k & \cos\theta_k \end{bmatrix}$$

also, the kinetic energy of the rotating blade takes the following form:

$$T = \frac{1}{2} \sum_{k=1}^{n} \int_V \rho V . V \, dV \quad \ldots(22)$$

to derive the governing equation of motion, an extended Hamilton's principle is used as;

$$\int_{t_o}^{t_1} (\delta T - \delta U) dt = 0 \quad \ldots(23)$$

The variation on the strain energy U and kinetic energy T can be written as;

$$\delta U = \int_V \begin{bmatrix} \delta\varepsilon_{xx} E \varepsilon_{xx} + \delta\varepsilon_{yy} E \varepsilon_{yy} + \delta\gamma_{xy} G \gamma_{xy} + \\ \delta\gamma_{yz} G \gamma_{yz} + \delta\gamma_{xz} G \gamma_{xz} \end{bmatrix} dV \quad \ldots(24)$$

$$\delta T = -\int_V \rho \left\{ \overline{P}_u \ \delta u + \overline{P}_v \ \delta v + \overline{P}_w \ \delta w \right\} dV \quad \ldots(25)$$

hence, the governing equations are derived as;

$$M \ddot{q} + C \dot{q} + (K_1 + K_g + K_{cf}) q = F_{cf} \quad \ldots(26)$$

where M, C, K_l and K_g are the mass matrix, the Coriolis matrix, the linear stiffness matrix and the geometric stiffness matrix, respectively. In addition, K_{cf} and F_{cf} are the stiffness matrix and the force vector due to the centrifugal force. For the dynamic analysis, the solution of eq. (26) is separated to the static and time dependent terms. Then the displacement vector q may be expressed as $q = q_s + \delta(t)$, where q_s and $\delta(t)$ denote the static solution and a small time dependent perturbation about the static equilibrium state, respectively. Thus, the perturbed equations can be obtained as follows;

$$M \ddot{\delta} + C \dot{\delta} + (K_1 + K_g + K_{cf}) \delta = 0 \quad \ldots(27)$$

To solve Eq. (27), it can be rewritten in the state space form,

$$Ag - B\dot{g} = 0 \quad \ldots(28)$$

Where,

$$A = \begin{bmatrix} M & 0 \\ 0 & K \end{bmatrix}, \quad B = \begin{bmatrix} 0 & M \\ -M & -C \end{bmatrix} \ and \ g = \begin{bmatrix} \dot{\delta} & \delta \end{bmatrix}^T$$

The solution of Eq. (28) is assumed to be of the form $g = C e^{\lambda t}$, where C is an arbitrary constant. As a result, the equation of motion can be simplified as a generalized eigenvalue problem in the form of:

$$Ag = \lambda B g \quad \ldots(29)$$

3. Case Study

The stresses and vibration characteristics effect on the blade caused by the centrifugal forces are investigated for two models of blades and three damaged cases. The models have the same properties and dimensions except fiber orientations.

The following material properties of Graphite/Epoxy were used in the numerical study. Basically, it is assumed that the layers are perfectly bonded together and the width of the models is (W=٠.٣٠٥ m). The laminated sheet is symmetric about the mid-plane with a stacking sequence of $[(0/90)_4]_s$ for the first model and $[(45/-45)_4]_s$ for the second model.

The shell element used in this analysis is three dimensional with six degrees of freedom for each node and the stresses and frequencies are computed for different mesh; it is preferable to suitable mesh size to be used during the analysis [No. of elements for (L/W=1, 225 elements), (L/W=2, 450 elements), (L/W=3, 675 elements) & (L/W=4, 900 elements)]. In each of the simulations, the blade constrained from one edge and frees from the other edges of the plate. The boundary conditions are shown in Fig. (4).

Elastic modulus	E_{11} = 98:0 GPa, E_{22} =7.9 GPa
Shear modulus	$G_{12}=G_{13}= G_{23}$=5.6 GPa
Density	$\rho = 1520 Kg / m^3$
Poisson's ratio	$\upsilon_{12} = 0.28$
Number of layers	8
Ply thickness	0.381 mm

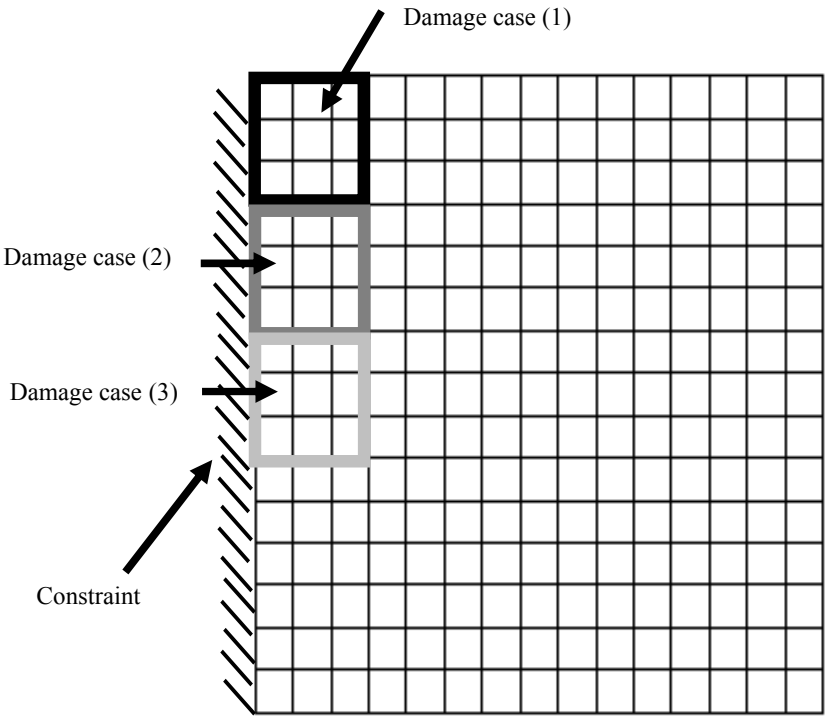

Fig.4-a. The Boundary Conditions and Damage Locations for Two Models (L/W=1, No. of Elements=225).

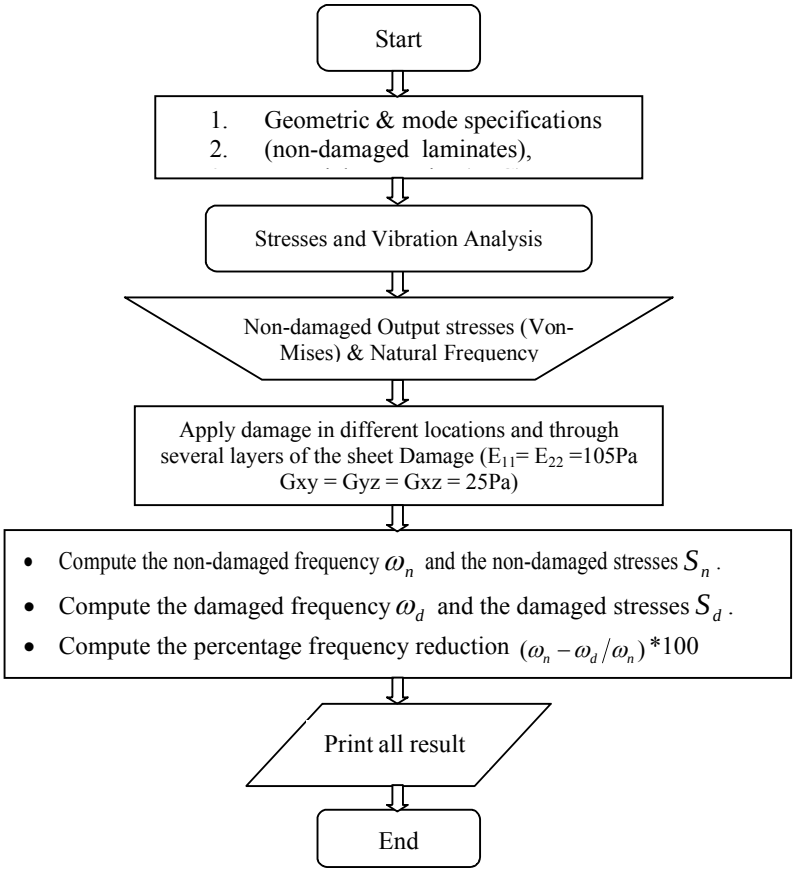

Fig.4-b. The Typical Block Diagram of the Present Stresses Increases and Frequencies Reduction for the Damaged Composite Blades.

4. Simulation of Damage

The method used to simulate damage in the composite models was to assume that the modulus and shear modulus were nearly zero at the location of damage. In order to avoid singularity issues during calculation, the properties were not set exactly to zero. For all damage cases, the material properties assigned to that location were as follows:

E11= E_{22} =105Pa
Gxy = Gyz = Gxz = 25Pa

The values of these properties actually are neglected (very small values greater than zero) compared with non-damaged structure. The strength in damaged regions is decreased by a factor of 10^8, which essentially acts as zero. These properties represent the effect of a total failure of the load carrying capability of that region. The initial effects of damage are difficult to model. For example no stiffness reduction is assumed after primary matrix failure occurs because transverse matrix cracks alone usually do not have a significant effect on the laminate stiffness.

The damage locations are shown in Fig. (4). In this figure, the squares represent the regions in which damage occurs. The details of each the damage case is outlined in Table (1).

Table 1,
Description of the Damage Cases.

Damage Case	Description of Damage Cases
1	A 3x3 region of elements in the top left corner of the blade with layers (3 to 6) failed, and layers (1 to 2) and (7 to 8) non-damaged.
2	A 3x3 region of elements in the left side with layers (3 to 6) failed, and layers (1 to 2) and (7 to 8) non-damaged.
3	A 3x3 region of elements in the center left side of the plate, with layers (3 to 6) failed, and layers (1 to 2) and (7 to 8) non-damaged.

5. Verification Test

In order to verify the program, the natural frequencies are calculated; then compared with the results of Ref. [19] and Ref. [20]. The comparison results are presented in Tables (2.a and 2.b). From Tables (2.a and 2.b), it is observed that a good agreement between the present calculated results and the results of references has been obtained. . In these tables the maximum error does not exceeds 1.84 %.

The data for the verification case [for Table (2.a)] are:

$$E = 217Gpa,\quad a = 328mm,\quad \rho = 7850 Kg/m^3,$$

$$Speed = 100\pi\ rad/\sec,\quad t = 3mm,\quad b = 28mm,$$

$$\upsilon = 0.3,\qquad r = 150mm$$

The data for the verification case [for Table (2.b)] are:

$$E_x = 43.3Gpa, E_Y = 12.7Gpa, E_Z = 12.7Gpa, \nu_{xy} = 0.29$$

$$, \nu_{yz} = 0.5, , \nu_{xz} = 0.29 G_{xy} = 4.5Gpa, G_{yz} = 2Gpa, G_{xz} = 4.5Gpa,$$

$$\rho = 1800 Kg/m^3, a = 1.219m, b = 0.914m, t = 0.00635m$$

$$t(for\ each\ ply) = 0.000317m$$

20-ply composite with S2 Glass /Epoxy symmetric $[(0/90)_{10}]$, Defect area =0.1875*0.1828 [location in the center of sheet with layers (4 to 13) failed]. All edges for sheet are fixed. Distributed load over an area 0.0247 m^2 (circle in the center of sheet with diameter 0.1774 m) of with a magnitude 2500 N (the total force on the sheet).

Table 2.a,
Values of Fundamental Natural Frequency (Hz) for Stationary and Rotating Cantilever Plate.

	Present Work	Ref. [19]	Error %
$(\Omega = 0)$	23.9	23.6	1.2
$(\Omega = 100\pi\ rad/\sec)$	52.9	52.0	1.8

Table 2.b,
Values of the First Five Natural Frequencies (Hz) for Damaged Rectangular Composite Sheet.

Mode No.	Present Work	Ref. [20]	Error %
1	36.22	36.52	0.82
2	62.15	62.74	0.94
3	86.24	86.89	0.74
4	105.15	105.95	0.75
5	106.2	107.09	0.83

6. Study State Analysis

Many parameters are investigated in this analysis; non-dimensional speed, aspect ratio, skew angle, pre-twisted angle and non-dimensional radius. The calculating frequencies of the cracked plated precede the proposed block diagram in Fig. (3).

a) Effect of Rotational Speed

The variations of Von-Mises stresses with non-dimensional speed (Ω=0.25, 0.5, 0.75 & 1) for two models of damaged composite blade is compared with non-damaged composite blade. For the first model (The laminated sheet is symmetric about the mid-plane with a stacking sequence of $[(0/90)_4]_s$). Fig.(5) shows the variations of Von-misses stresses with Ω. In this figure, it was observed that the stresses increase when the speed of rotation increased too.

The behavior for stresses with Ω is the same for the second model (The laminated sheet is symmetric about the mid-plane with a stacking sequence of $[(45/-45)_4]_s$). Fig.(6) exhibits the variations of Von- misses stresses with Ω.

Generally the stresses are proportional with speed of rotation and the stresses will be increased for damaged blades compared with the non-damaged blade. When (Ω=1) the percentage increases in Von-misses stresses for the first model of damaged blade is 69.7% and for the second model of damaged blade is 50.8% in comparison with the non-damaged blades.

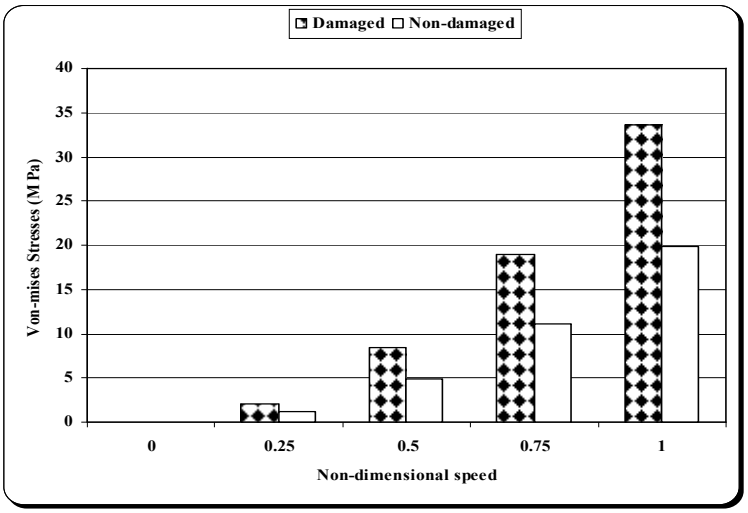

Fig.5. Variation of Von-Mises Stresses with Ω (1st Model, L/W=1, $\theta = 0, \bar{r} = 1, \alpha = 0$).

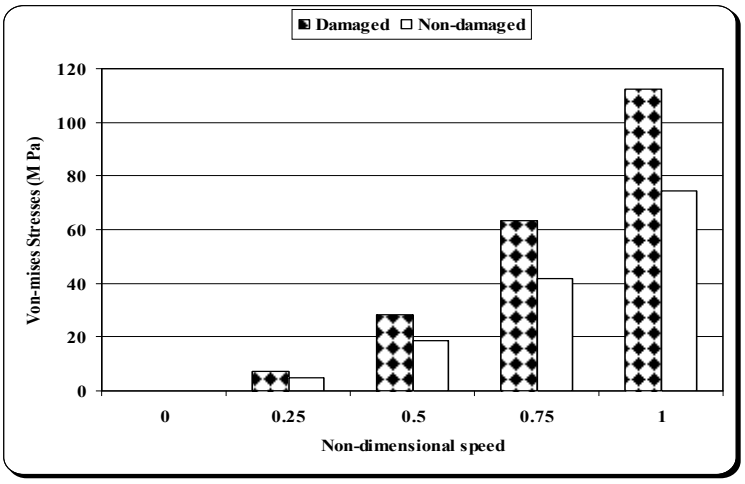

Fig. (6) Variation of Von-Mises Stresses with Ω (2nd Model, L/W=1, $\theta = 0, \bar{r} = 1, \alpha = 0$).

b) Effect of Aspect Ratio

In order to investigate the aspect ratio of blade, four aspect ratios (1, 2, 3 & 4) were selected for this investigation.

Figs. (7 & 8) show the variations of Von-misses stresses with aspect ratio for the first model and the second model respectively.

When (L/W=1), the percentage increases in Von-misses stresses for first model of damaged blade to be 69.5% and for the second model of damaged blade it because 50.8% in comparison with the non-damaged blade.

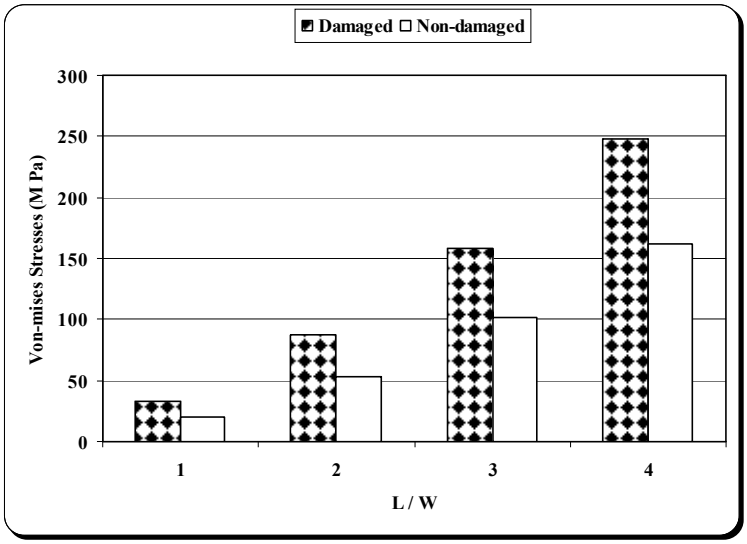

Fig.7. Variation of Von-Mises Stresses with (L/W) (1st Model, Ω=1, $\theta = 0, \bar{r} = 1, \alpha = 0$).

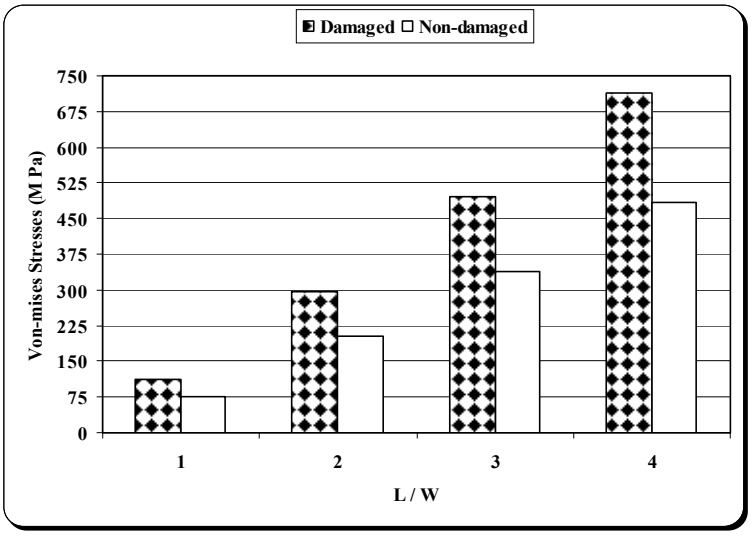

Fig.8. Variation of Von-Mises Stresses with (L/W) (2nd Model, Ω=1, $\theta = 0, \bar{r} = 1, \alpha = 0$).

c) Effect of Skew Angle

Also the stresses computed for the same models of damaged composite blades have different combination of skew angles (0^o, 10^o, 20^o, 30^o, 40^o, and 45^o).

Figs. (9 & 10) exhibit the variation of Von-misses stresses with skew angle for the first model and the second model respectively.

It has been shown that, the maximum Von-misses stresses occur at 45^o skew angle for all cases.

When the skew angles is (0^o), the percentage increases in Von-misses stresses for first model of damaged blade to be 69.7% and for the second model of damaged blade it becomes 50.8% in comparison with the non-damaged blades.

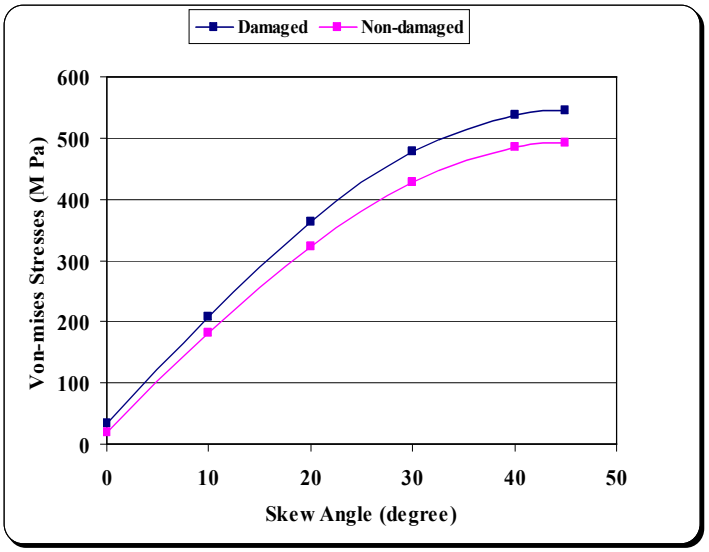

Fig.9. Variation of Von-Mises Stresses with skew angle (2nd Model, Ω=1, L/W=1, $\bar{r} = 1, \alpha = 0$).

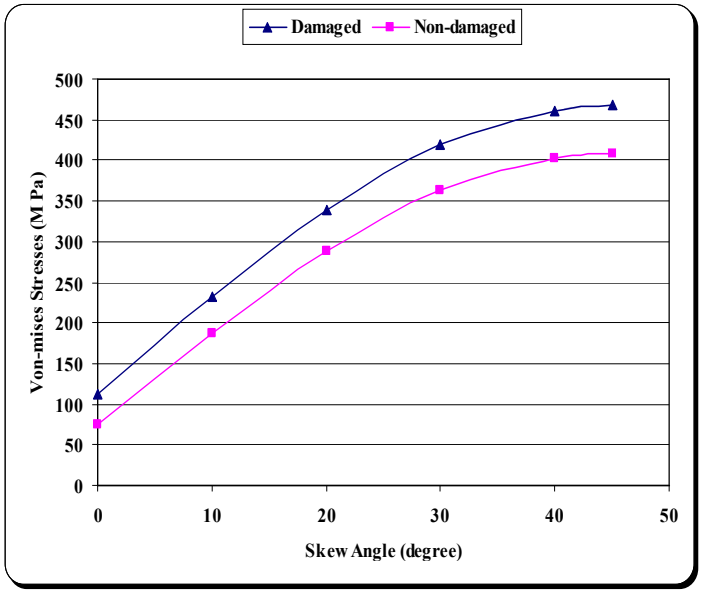

Fig.10. Variation of Von-Mises Stresses with Skew Angle (1st Model, Ω=1, L/W=1, $\bar{r} = 1, \alpha = 0$).

d) Effect of Pre-Twist Angle

The study covers the effects of four pre-twist angles (0^o, 15^o, 30^o and 45^o) on Von-misses stresses.

Figs. (11 &12) show the variations Von-misses stresses with pre-twist angle for the first model and the second model respectively.

It can be observed that when the pre-twist angle increases, the stress increases too.

The pre-twist of the blade causes coupling in both bending directions. Hence, the pre-twist angle must be kept to minimum gross. Untwisting can cause changes in the velocity triangles of the fluid flow; leading and trailing edge tip clearance can change drastically due to blade untwist; and both effects cause degradation in turbomachine performance. Bearing in mind, fluid dynamic requirement of pre-twist angle is to achieve maximum efficiency and minimum stress level.

It can be noted from the previous figures that, when pre-twist angle is (45^o), the percentage increases in Von-misses stresses to be (33.8% and 30.4%) for first and second models respectively, in comparison with the non-damaged blades.

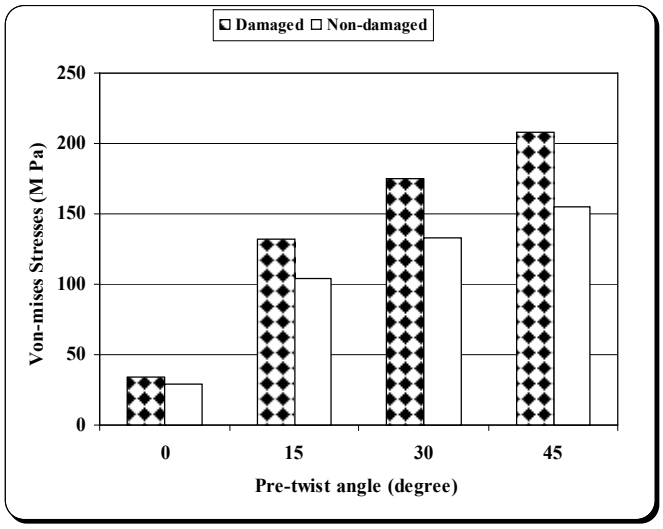

Fig.11. Variation of Von-Mises Stresses With Pre-Twist Angle (1st Model, Ω=1, L/W=1, $\bar{r}=1, \theta=0$).

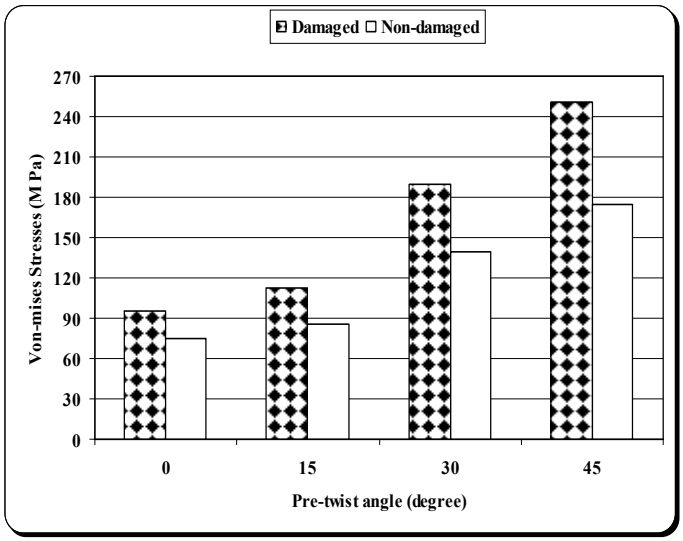

Fig.12. Variation of Von-Mises Stresses With Pre-Twist Angle (2nd Model, Ω=1, L/W=1, $\bar{r}=1, \theta=0$).

e) Effect of Disc Radius

Figs. (13 & 14) demonstrate the variations of Von-mises stresses with non-dimensional radius of disc (R/L).

It can be observed the disc radius is the effect of the large part of results, which the natural frequencies are proportional to the speed of rotation and disc radius. It was observed that the stresses increase when the disc of radius increased too. And the maximum percentage increases in Von-misses stresses to be (73.9% and 59.2%) for the first model and the second model respectively in comparison with the non-damaged blades.

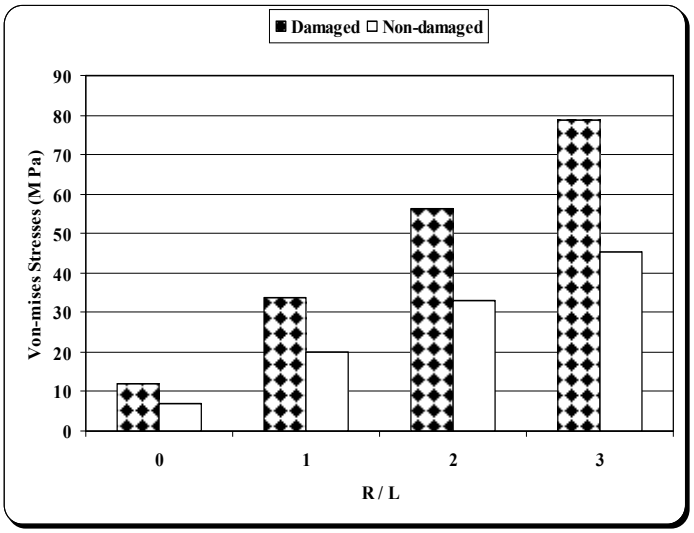

Fig.13. Variation of Von-Mises Stresses With (R/L) [1st Model, Ω=1, L/W=1, $\alpha = 0$, $\theta = 0$].

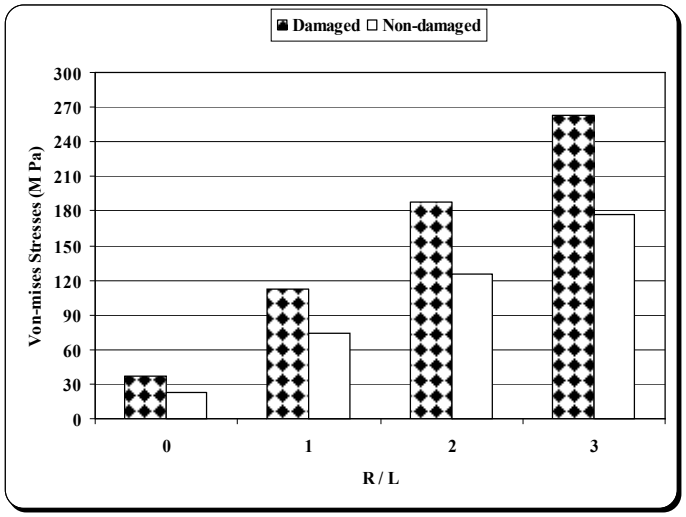

Fig.14. Variation of Von-Mises Stresses With (R/L) (2nd Model, Ω=1, L/W=1, $\alpha = 0$, $\theta = 0$).

7. Vibration Analysis

In this part the effect of damaged for composite blade on the vibration characteristics is investigated. And for the same parameters in section (6).

Figs. (15, 17, 19, 21 & 23) show the variation of Fundamental Natural Frequency with non-dimensional speed, aspect ratio, skew angle, pre-

twisted angle and non-dimensional radius respectively, for the first model.

Figs. (16, 18, 20, 22 & 24) demonstrate the variation of Fundamental Natural Frequency with non-dimensional speed, aspect ratio, skew angle, pre-twisted angle and non-dimensional radius respectively, for the second model.

The numerical results in Tables. (3 & 4) show the first five natural frequencies for the composite blade (non-damaged case and damaged cases) for the first model and second model respectively.

It can be noticed that all values of the natural frequencies increase with the speed of rotation and with the increasing radius of the disc [For this case when, the speed of rotation and disc radius increases, the values of centrifugal force increases also; then, the stiffness values for structure will increase by depending on Equation (26) and the resultant for the values of frequencies will increases]. An increase in the pre-twist angle and setting angle causes a decrease in the natural frequencies. It can be recognized that when the aspect ratio increase the natural frequencies decreases [For this case when the aspect ratio increases the value of mass for the structure increases also and the resultant for the values of frequencies will decreases]. It can be observed that the speed of rotation and disc radius aeffect the large part of results; the natural frequencies are proportional to the speed of rotation and disc radius. Also, the small difference in natural frequencies between the damage cases and non-damaged case can be noted. The maximum difference percentage does not exceed 2.1 %, because of the small damage.

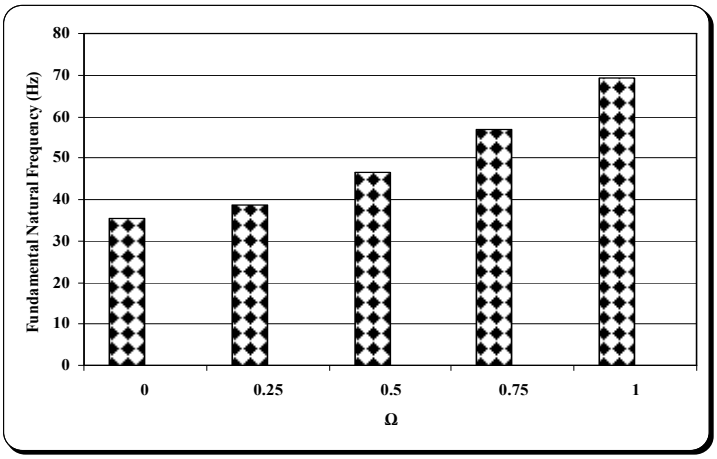

Fig.15. Variation of Fundamental Natural Frequency (Hz) with Non-Dimensional Speed (1st Model, L/W=1, $\theta = 0, \bar{r} = 1, \alpha = 0$).

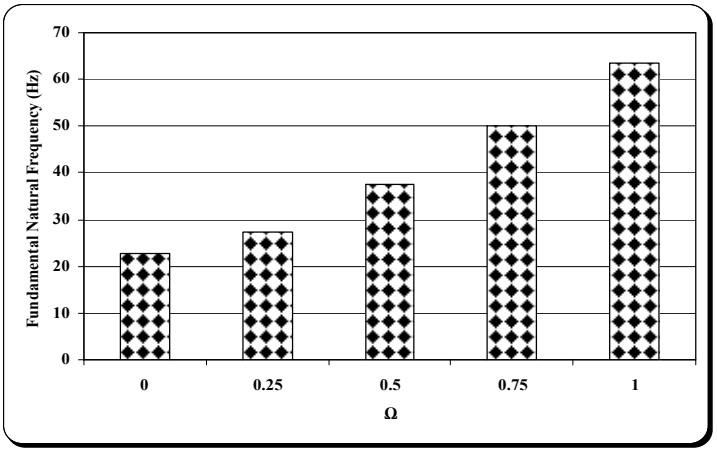

Fig.16. Variation of Fundamental Natural Frequency (Hz) with Non-Dimensional Speed (2nd Model, L/W=1, $\theta = 0, \bar{r} = 1, \alpha = 0$).

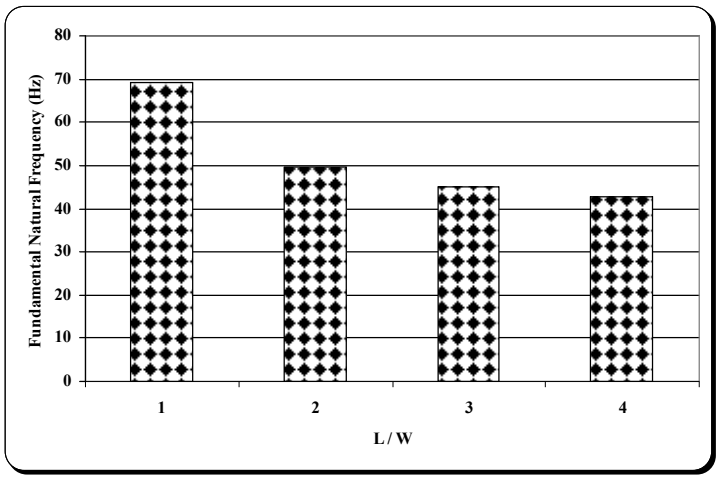

Fig.17. Variation of Fundamental Natural Frequency (Hz) with (L/W) (1st Model, Ω=1, $\theta = 0, \bar{r} = 1, \alpha = 0$).

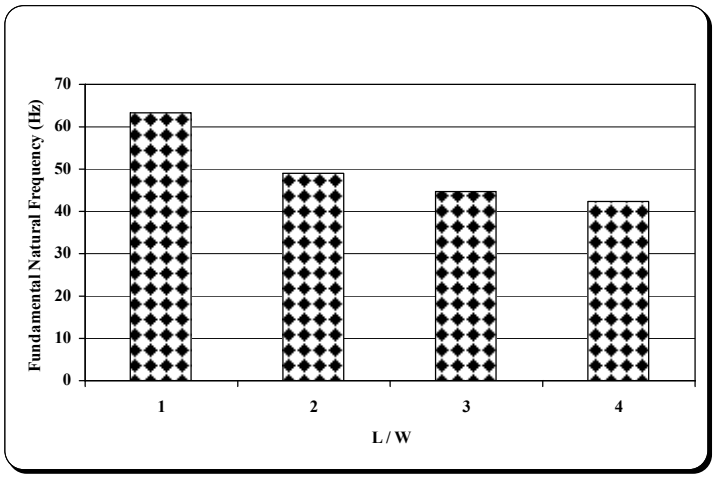

Fig.18. Variation Fundamental Natural Frequency (Hz) with (L/W) (2nd Model, Ω=1, $\theta = 0, \bar{r} = 1, \alpha = 0$).

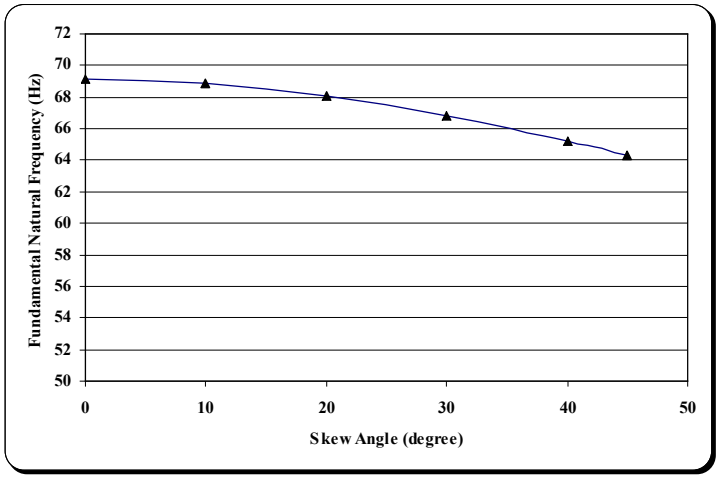

Fig.19. Variation of Fundamental Natural Frequency (Hz) with Skew Angle (1st Model, Ω=1, L/W=1, $\bar{r} = 1, \alpha = 0$).

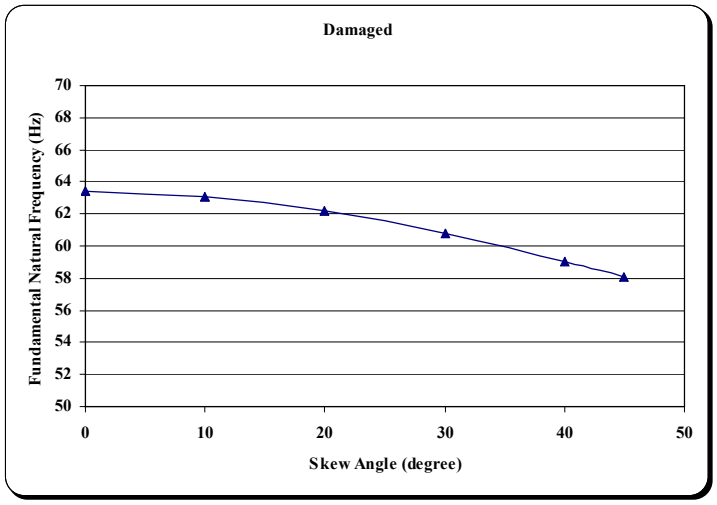

Fig.20. Variation of Fundamental Natural Frequency (Hz) with Skew Angle (2nd Model, Ω=1, L/W=1, $\bar{r}=1,\alpha=0$).

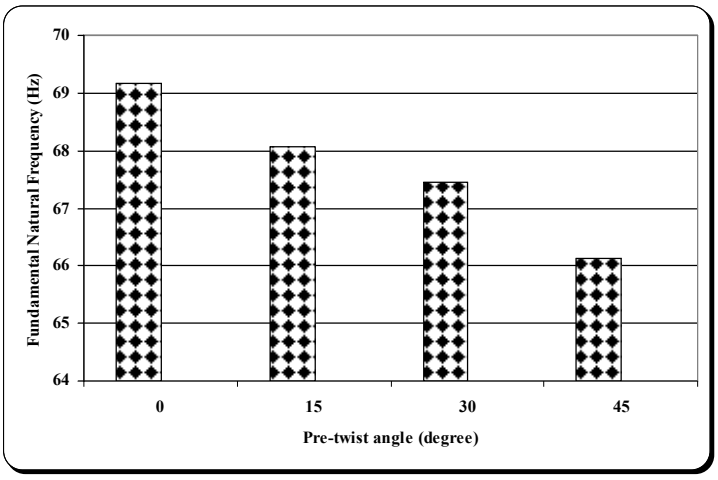

Fig.21. Variation of Fundamental Natural Frequency (Hz) with Pre-Twist Angle (1st Model, Ω=1, L/W=1, $\bar{r}=1,\theta=0$).

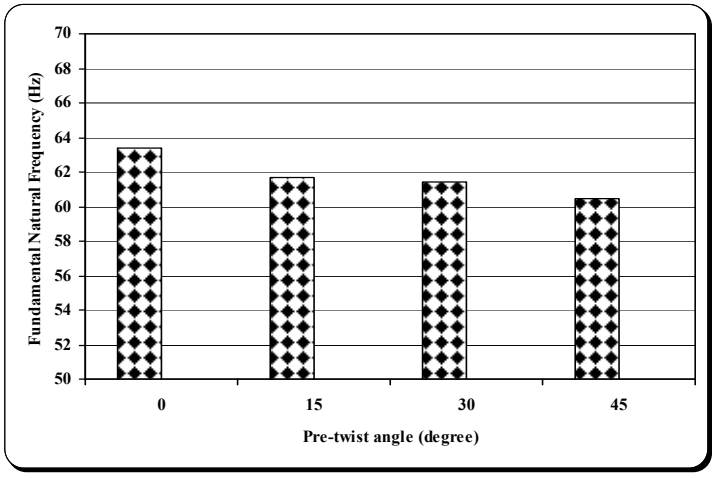

Fig.22. Variation of Fundamental Natural Frequency (Hz) with Pre-Twist Angle (2nd Model, Ω=1, L/W=1, $\bar{r}=1,\theta=0$).

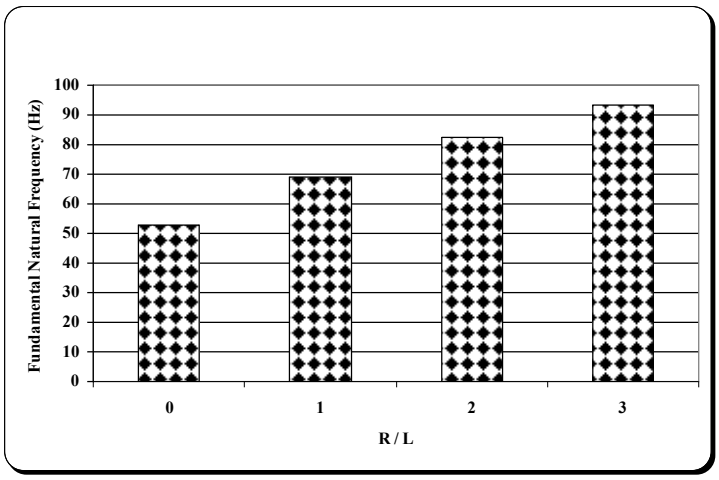

Fig.23. Variation of Fundamental Natural Frequency (Hz) with (R/L) [1st Model, Ω=1, L/W=1, $\alpha = 0,\ \theta = 0$]

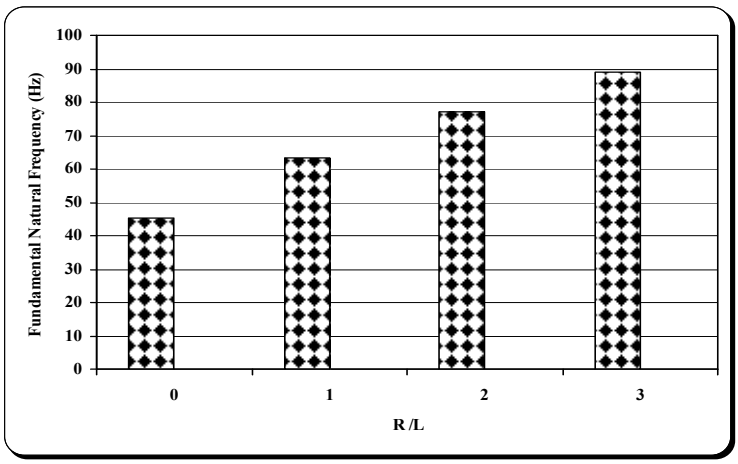

Fig.24. Variation of Fundamental Natural Frequency (Hz) with (R/L) (2nd Model, Ω=1, L/W=1, $\alpha = 0,\ \theta = 0$).

Table 3,
Values of the First Five Natural Frequencies (Hz) for the Composite Blade (Non-Damaged Case and Damaged Cases for 1st Model).

Mode No.	Non-damaged Case	Case (1)	%Difference Case (1) With Non-damaged case	Case (2)	%Difference Case (2) With Non-damaged case	Case (3)	%Difference Case (3) With Non-damaged case
1	36.14	35.58	1.54	35.59	1.51	35.596	1.50
2	54.32	53.55	1.43	53.64	1.26	53.768	1.03
3	187.16	184.02	1.68	184.25	1.55	184.27	1.54
4	227.01	223.66	1.47	223.69	1.46	223.69	1.46
5	251.31	247.73	1.42	248.46	1.13	248.12	1.27

Table 4,
Values of the First Five Natural Frequencies (Hz) for the Composite Plate (Non-Damaged Case and Damaged Cases for 2nd Model).

Mode No.	Non-damaged Case	Case (1)	%Difference Case (1) With Non-damaged case	Case (2)	%Difference Case (2) With Non-damaged case	Case (3)	%Difference Case (3) With Non-damaged case
1	23.2	22.700	2.15	22.718	2.07	22.746	1.95
2	78.34	76.773	2.00	76.991	1.72	76.951	1.77
3	137.1	134.33	2.02	134.80	1.6	134.85	1.64
4	210.24	205.94	2.04	205.97	2.03	206.06	1.98
5	262.32	256.86	2.08	257.06	2.00	257.02	2.02

8. Conclusions & Recommendations

The conclusions obtained from the present work can be summarized as follows: -

1. The frequencies of all modes of vibration are independent of skew angle and disc radius when the cantilever plate (blade) is stationary. But the effects of skew angle and disc radius will be very clear, when the blade start to rotate. The maximum percentage increases in Frequencies to be (99.5% and 186 %) for the first model and the second model respectively, when the non-dimensional speed changes from zero to 1.
2. The maximum effect of skew angle and pre-twisted angle on the values of natural frequencies occurs when angles are $\left(\theta = \alpha = 0^{\circ}\right)$. The maximum percentage increases in Frequencies to be (17% and 8.6 %) for the first model and the second model respectively, when the skew angle change from 45 to zero. And the maximum percentage increases in Frequencies to be (3% and 4.6 %) for the first model and the second model respectively, when the pre-twisted angle changes from 45 to zero.
3. The maximum effect of skew angle and pre-twisted angle on the values of stresses occurs when angles are $\left(\theta = \alpha = 45^{\circ}\right)$.
4. The speed of rotation and disc radius are very effective parameters on the frequencies and stresses for rotating blades (Blades design needs to high accuracy estimation for the stresses and frequencies, and using the optimization to select materials and others design parameters such as skew and per-twisted angles, thickness, aspect ratio etc.. before manufacturing).
5. It can be noted, the stresses in all cases for the second model of blade larger than the first model under same conditions, in the other words, It can be concluded the great effect of fiber orientation of composite blade for the same damage (size and location). In this work, two types of fibers orientations have been used to make Comparison and to show the high difference for stresses under the same conditions.

Because of the small damage or invisible damage, which causes the high stresses in blade, this may lead to the failure. Finally, the important recommendation here for the future work is using high accuracy devices to get the natural frequencies values, to discover the small and invisible damage in the blade and using the optimization method to select the parameters such as (orientations of fibers for composite materials, thickness, skew angle, Pre-twist angle etc..)

Notations

U	The displacement vector
u_0, v_0, w_0	Three translational displacement
α, β	The two rotational degrees of freedom
N	The interpolation function matrix
ε	the strain
B_{st}	The complete structural strain–displacement matrix
U	The strain energy
Ω	Non-dimensional speed
E	The modules of elasticity (N/m^2)
G	The modules of rigidity (N/m2)
Ttw	is the coordinate transformation matrix for a blade twist

T	The kinetic energy
M	The mass matrix
C	The Coriolis matrix
Kl	The linear stiffness matrix
Kg	The geometric stiffness matrix
Kcf	The stiffness matrix due to the centrifugal force
Fcf	force vector due to the centrifugal force
q	The displacement vector q

9. References

[1] V.Omprakash and V. Ramamurti, "Dynamic stress analysis of rotating turbomachinery Bladed-Disc systems", J. of Computers and structures, Vol. 32, No. 2, PP. 477-488, 1989.

[2] N. G. Stephen and P. J. Wang, "Stretching and bending of rotating beam", J. of Applied Mechanics, Transactions of the ASME, Vol. 53, PP. 869-872, December 1986.

[3] Leissa AW, Ewing MS. "Comparison of beam and shell theories for the vibrations of thin turbomachinery blades", J. Eng Power 1983; 105: 383–92.

[4] Dokainish MA, Rawtani S. "Vibration analysis of rotating cantilevered plates", Int. J. Numer. Meth. Eng. 1971;3: 233–48.

[5] Ramamurti V, Kielb R. "Natural frequencies of twisted rotating plates", J. Sound Vib 1984 ;97(3):429–49.

[6] Leissa AW, Lee JK, Huang AJ. "Vibrations of cantilevered cylindrical shallow shells having rectangular planform" J. Sound Vib 1981;78(3):311–28.

[7] Leissa AW, Lee JK, Wang AJ. "Rotating blade vibration analysis using shells", J. Eng Power 1982;104: 296–302.

[8] Leissa AW, Lee JK, Huang AJ. "Vibrations of cantilevered doublycurved shallow shells", Int. J. Solids Struct 1983; 19 (5): 411–24.

[9] Leissa AW, Lee JK, Huang AJ. "Vibrations of twisted rotating blades", ASME J. Vib Acoust Stress Reliability Des 1984; 106(2):251–7.

[10] Henry TY, Masud A, Kapania RK. "A survey of recent shell finite elements", Int. J. Numer Meth Eng 2000;47:101–27.

[11] Sohrabuddin Ahmad, Irons BruceM, Zienkiewicz OC. "Analysis of thick and thin shell structures by curved finite elements" Int. J. Numer Meth Eng 1970;2:419–51.

[12] Ramm E. "A plate/shell element for large deflections and rotations" In: Bathe KJ, editor. Formulations and computational algorithms in finite element analysis. Cambridge, MA: MIT press; 1977.

[13] Bathe KB, Bolourchi S. "A geometric and material nonlinear plate and shell element", Comput Struct 1980;11: 23–48.

[14] Huang HC, Hinton E. "A new nine node degenerated shell element with enhanced membrane and shear interpolation", Int. J. Numer Meth Eng 1986; 22:73–92.

[15] Lee SJ, Han SE. "Free vibration analysis of plates and shells with a nine-node assumed natural degenerated shell element", J. Sound Vib 2001; 241(4):605–33.

[16] Bhumbla R, Kosmatka JB, Reddy JN. "Free vibration behavior of spinning shear-deformable plates composed of composite materials", AIAA J. 1990; 28(11):1962–70.

[17] Lam KY, Qian W. "Vibration of thick rotating laminated composite cylindrical shells", J. Sound Vib 1999;225(3):483–501.

[18] Prema Kumar WP, "Palaninathan R. Finite element analysis of laminated shells with exact through-thickness integration", Comput Struct 1997;63(1):173–84.

[19] Young-Jung Kee & Ji-Hwan Kim, "Vibration characteristics of initially twisted rotating shell type composite blades", J. Composite Structures, (2004), 64, pp 151–1.

[20] Abdullah O. Ibraheem, Ehsan M. Z and Wassan Safaa, "A finite Element Analysis of Damaged Composite Sheet", Engineering & Development (College of Engineering/ Al-Mustansiriya University), Vol. 12, No. 4, December (2008).

التحليل باستخدام نظرية العناصر المحددة لريشة مركبة دوارة متضررة

عدي أبراهيم عبدالله
قسم هندسة الطاقة/ كلية الهندسة/ جامعة بغداد
البريد الالكتروني: Odayia2006@yahoo.com
!! !! !

الخلاصة

في هذه البحث تم استخدام نظرية العناصر المحددة لدراسة السلوك الديناميكي لريشة مركبة دوارة متضررة. طور برنامج للعناصر المحددة ثلاثي الأبعاد باستعمال العنصر الموقوف الذي يحتوي على ثمانية عقد كعنصر تجزئة لهيكل الريشة الدوار. تم استخدام نفس نوع العنصر للريشة المتضررة والغير متضررة. في هذا التحليل تم أخذ تأثير الإجهاد الأولي (الجسأة الهندسية) والتأثيرات الدوبريلتي يؤخذ بنظر الاعتبار وجود تأثير التعجيل كوريولس (carioles acceleration). يظهر التحقيق تأثير عدة متغيرات مثل السرعة الدوران وسبة الطول للعرض وزاوية التثبيت وزاوية الميل و نصف قطر إلى الطول وطبقات التصفيح واتجاهه الليف للمادة المركبة. عملية النمذجة للريشة المركبة الدوارة الغير متضررة تم تطبيق حالات ضرر مختلفة لحساب التغير في قيمة التردد الطبيعي الأساسي الاتجاهات نسبة الى الريشة التي لا تحتوي على ضرر. تحدث الضرر في عدة طبقات لصفيحة المركبة في مواقع مختلفة خلال الحجم، وخلال عدّة طبقات للصفيحة. النَتائج العددية بينت توافق جيد بالمقارنة بالبحوث المتوفرة التي تَستعملُ طرقَ اخرى.